Environmental Science Nano

Nanoparticle surface charge influences translocation and leaf distribution in vascular plants with contrasting anatomy

Journal:	*Environmental Science: Nano*
Manuscript ID	EN-ART-06-2019-000626
Article Type:	Paper
Date Submitted by the Author:	04-Jun-2019
Complete List of Authors:	Spielman-Sun, Eleanor; Carnegie Mellon University, Civil and Environmental Engineering Avellan, Astrid; Carnegie Mellon University, Civil and Environmental Engineering Bland, Garret; Carnegie Mellon University, Department of Civil and Environmental Engineering Tappero, Ryan; Brookhaven National Laboratory, National Synchrotron Light Source II Acerbo, Alvin; Brookhaven National Laboratory, National Synchrotron Light Source II; University of Chicago, Center for Advanced Radiation Sources Unrine, Jason; University of Kentucky, Department of Plant and Soil Sciences Giraldo, Juan Pablo; UC Riverside, Department of Botany and Plant Sciences Lowry, Gregory; Carnegie Mellon University, Civil and Environmental Engineering

Nanoparticle surface charge influences translocation and leaf distribution in vascular plants with contrasting anatomy

Eleanor Spielman-Sun,[a] Astrid Avellan,[a] Garret Bland,[a] Ryan V. Tappero,[b] Alvin S. Acerbo,[bc] Jason M. Unrine,[d] Juan Pablo Giraldo,[e] Gregory V. Lowry*[a]

[a] Civil and Environmental Engineering, Carnegie Mellon University, Pittsburgh, Pennsylvania 15213, United States

[b] National Synchrotron Light Source II, Brookhaven National Laboratory, Upton, NY 11973, United States

[c] Center for Advanced Radiation Sources University of Chicago, Chicago, IL 60637, United States

[d] Department of Plant and Soil Sciences, University of Kentucky, Lexington, Kentucky 40546, United States

[e] Department of Botany and Plant Sciences, University of California, Riverside, CA 92521, United States

*Corresponding author:

Address: Carnegie Mellon University, Pittsburgh, PA 15213

Phone: (412) 268-2948

Email: glowry@cmu.edu

ABSTRACT

Root uptake and translocation of engineered nanoparticles (NPs) by plants is dependent on both plant species and NP physiochemical properties. To evaluate the influence of NP surface charge and differences in root structure and vasculature on cerium distribution and spatial distribution within plants, two monocotyledons (corn and rice) and two dicotyledons (tomato and lettuce) were exposed hydroponically to positively-charged, negatively-charged, and neutral ~4 nm CeO_2 NPs. Leaves were analyzed using synchrotron-based X-ray fluorescence microscopy to provide lateral Ce spatial distribution. Surface charge mediated CeO_2 NP interactions with roots for all plant species. Positively charged CeO_2 NPs associated to the roots more than the negatively charged NPs due to electrostatic attraction/repulsion to the negatively charged root surfaces, with the highest association for the tomato, likely due to higher root surface area. The positive NPs remained primarily adhered to the roots untransformed, while the neutral and negative NPs were more efficiently translocated from the roots to shoots. This translocation efficiency was highest for the tomato and lettuce compared to corn and rice. Across all plant species, the positive and neutral treatments resulted in the formation of Ce clusters outside of the main vasculature in the mesophyll, while the negative treatment resulted in Ce primarily in the main vasculature of the leaves. Comparing leaf vasculature, Ce was able to move much further outside of the main vasculature in the dicot plants than monocot plants, likely due to the larger airspace volume in dicot leaves compared to monocot leaves. These results provide valuable insight into the influence of plant structure and NP properties on metal transport and distribution of NPs in plants.

ENVIRONMENTAL SIGNIFIGANCE

Plant nanobiotechnology promises transformative solutions to the most vexing problems threatening global food security, e.g. drought, disease, and soil nutrient deficiencies. However, the lack of cost-effective methods to deliver the nanomaterials to precise locations in plants where they are needed to be active, e.g. inside vascular tissues, or into plant organelles, impedes these technological innovations. These findings not only provide insight into how plant structural features influence NP behavior but also how surface charge can be tailored for targeted delivery of nutrients to specific plant organs.

INTRODUCTION

Nanotechnology has the potential to become a valuable tool for improving agro-ecosystem resiliency against major environmental stressors (e.g. drought, salinity, disease) and efficiency by enhancing crop productivity and reducing nutrient losses (e.g. through controlled release of agrochemicals and target-specific delivery).[1–5] Firstly, nanoparticles (NPs) are mall enough to cross important plant mechanical barriers (e.g. cuticle and cell walls)[6]. NPs can also cross cellular and organelle membranes and move in between cells which enables them to load into the vasculature either via apoplastic (extracellular) or symplastic (intracellular) pathways, as both mechanisms have been proposed for translocation of NPs in plants.[4,7,8] Secondly, NP surfaces are easily modifiable with a variety of coatings and, similar to drug delivery, NP surface properties can theoretically be tuned to deliver them to specific tissues or organelles in plants.[9,10] Combined with the inherent rate limited dissolution of many metal and metal oxide NPs, NPs could provide inherent slow release[11,12] of the constituent metals in the desired locations of plants, which can be less phytotoxic than soluble forms of metals applied at the same dose.[13] Finally, NPs have been

shown to increase photosynthesis,[14,15] biomass production rates,[16,17] plant stress tolerance,[18] plant resistance to diseases,[19,20] and agrochemical utilization efficiency.[21] Despite the great potential of NPs, there remains limited understanding of how NP physical and chemical properties (e.g. size, charge, solubility, coating, chemical composition) dictate NP-plant interactions and translocation behavior in plants. A better understanding of these NP-plant interactions is needed to design targeted and controlled delivery, which has the potential to reduce the number of applications of fertilizers and pesticides, decrease nutrient losses from fertilizers, and increase yields through optimized nutrient management.

Surface charge is an important property dictating NP fate in plants. While positively-charged CeO_2 NPs have been shown to more readily attach to roots of wheat (*Triticum aestivum* cv. Shield) [22] and tomato (*Solanum lycopersicum* cv Micro-Tom),[23] negatively charged CeO_2 NPs more efficiently translocate to the shoots. The same trend has been observed for gold nanoparticles (AuNPs) in radish, ryegrass, rice and pumpkin[24] and in tomato and rice.[25] Because charge can influence NP interactions with charged biological structures[26] and therefore ability to cross biological membranes,[27] it is desirable to better understand precisely how charge affects the spatial distribution of NPs that have translocated in plants. Few studies characterize the spatial distribution of the NPs in leaves beyond total metal analysis, particularly at the whole-leaf scale.[(e.g.22,23,28)]

Though many published studies have focused on NP uptake by plant roots, the observations made in one plant species are often difficult to generalize to other plants. Often differences in the plant's structural features, e.g. root or leaf architecture, are hypothesized to explain the observed differences in NP uptake and translocation, but this hypothesis has yet to be systematically evaluated. Flowering plants (angiosperms) can be classified by anatomical differences into two

categories: monocotyledon (monocot) and dicotyledon (dicot). In general, monocots are more resistant to heavy metal NP uptake than dicots.[29–32] Differences in NP uptake between monocots and dicots could be due to differences in vasculature and structural features (fibrous vs taproot system) leading to different surface area interacting with the environment, greater binding capacity and transpiration[33] in dicots, and differences in root exudation profiles,[(e.g.34–37)] as well as mucilage production at the NPs-root tip interface.[38] However, the relative importance of each of these differences has yet to be thoroughly investigated.

CeO_2 NP interactions with different plant species have been widely studied. However, there are contradictory reports on whether CeO_2 NPs may act as oxidative stress inducer or antioxidant. CeO_2 NPs have been shown to protect cells *in vitro* against reactive oxygen species (ROS)-induced damage,[39–41] including isolated chloroplasts[14,42] due to oxygen vacancies in the crystalline lattice that readily enable cycling between Ce^{3+} and Ce^{4+} oxidation states. However, there are limited examples of this potential *in vivo*. CeO_2 NPs with low Ce(III)/Ce(IV) ratios (50 mg/L) delivered via foliar infiltration have also been shown to improve plant photosynthetic rates under heat[43] and salinity[18,44] by serving as antioxidants. In contrast, decreased photosynthetic rate and CO_2 assimilation efficiency, increased lipid peroxidation, and other stress measures have also been observed in a variety of plants exposed to CeO_2 NPs, particularly at high doses greater than 500 mg/kg soil[(eg. 45–49)] and NPs with higher Ce(III)/Ce(IV) ratios.[(eg. 50)] A better understanding of the impacts of NP properties on plant photosynthesis and respiration is needed to fully leverage their benefits.

The goal of the present study was to systematically assess whether plants with different morphologies, two monocots (corn and rice) and two dicots (tomato and lettuce) similarly accumulate CeO_2 NPs and how NP charge influences spatial distribution in leaves with

contrasting architectures. We use short-term, well-controlled hydroponic exposure scenarios to determine whether differences in NP charge and plant anatomy and physiology influence the translocation, speciation changes, and spatial distribution of Ce within the plant leaf tissue. A better understanding of the impact of NP charge on translocation routes and distribution in leaves can inform future efforts to design NPs for delivery to specific locations in plant tissues.

MATERIALS AND METHODS

Material Characterization: Cerium dioxide NPs with three different charges were synthesized as reported previously in Collin et al.[51] Briefly, uncharged dextran coated CeO_2 NPs (CeO_2 NP (0)) with a nominal 4 nm primary particle diameter were synthesized then further functionalized with either diethylaminoethyl groups to create a net positive charge (CeO_2 (+)) or with carboxymethyl groups to create a net negative charge (CeO_2 (−)). The particles were diluted to 50 mg/L as Ce in a basal salt solution (1 mM $CaCl_2$ and 5 μM H_3BO_3, pH=5.6) and probe sonicated (550 Sonic Dismembrator, Fisher Scientific) for 1 min at 10 s intervals to ensure dispersion. The hydrodynamic diameter and electrophoretic mobility of the NPs in the exposure medium at the exposure concentration (50 mg-Ce/L) were measured using a Nano Zetasizer (Malvern Instruments, Malvern).

Plant Growth and Exposure: Crops commonly grown in the United States and easy to cultivate in lab were chosen as model plants. Corn (*Zea mays* cv. *Trinity*) and lettuce (*Lactuca sativa* cv. *Buttercrunch*) seeds were obtained from Johnny's Selected Seeds (Winslow, ME), and tomato (*Solanum lycopersicum* cv. *Roma*) from Burpee Seeds (Warminster, PA). Rice (*Oryza sativa* cv. *Nipponbare*) were obtained from the USDA-ARS Dale Bumpers National Rice Research Center (Stuggart, AR). Seeds were surface sterilized with commercial bleach for 10 min and then

thoroughly rinsed with DI water. The sterilized seeds were germinated on deionized water-moistened filter paper in a Petri dish for 4 days for corn, 6 days for tomato and lettuce, and 7 days for rice. Germination was staggered so that all plants were transferred to hydroponic containers on the same day. Each 100-mL container was filled with 80 mL of ¼ strength Hoagland's medium and covered with a plastic lid with five holes. Five seedlings were transplanted to five of the holes with the roots suspended in a continuously aerated solution. Plants were grown in a controlled environment chamber (Binder™ Model KBWF 729; day/night photoperiod 16h/8h, day/night temperature 25 °C /21 °C and 60% humidity). Solution was renewed every 3 days with fresh ¼ strength Hoagland's medium. After 2 weeks, the plants were hydroponically exposed to 50 mg-Ce/L of CeO_2 NPs as $CeO_2(+)$, $CeO_2(0)$, or $CeO_2(-)$ in a continuously aerated basal salt solution (1 mM $CaCl_2$ and 5 μM H_3BO_3, pH=5.6) for 48 h. Exposures were performed in this solution to reduce phosphate interference[52] and over a short period of time to focus on the plant's initial response to particles with different charges. After exposure, plant roots were rinsed for 30 s in Ce-free medium to remove loosely adhered Ce. This exposure protocol was used for all subsequent measurements.

Plant Health Measurements: At the end of the 48 h exposure period, photosynthetic CO_2 quantum yield (ΦCO_2; $\mu mol_{CO2} \cdot \mu mol_{photon}^{-1}$), photosystem II quantum yield ($\Phi PSII$; mol $e^- \cdot \mu mol^{-1}$), transpiration rates (E; $mol_{H2O} \cdot m^{-2} \cdot s^{-1}$), electron transport rates (ETR; $\mu mol_{photon} \cdot m^{-2} \cdot s^{-1}$), and stomatal conductance (gsw; H_2O $mol \cdot m^{-2} \cdot s^{-1}$) were measured in quadruplicate on light-adapted leaves using a LI-6800 portable gas analyzer and fluorometer (Li-COR Bio-sciences, Lincoln, NE). The leaf chamber conditions were: light intensity 600 $\mu mol \cdot m^{-2} \cdot s^{-1}$ Photosynthetically Active Radiation (PAR), humidity 60%, leaf temperature 25 °C, flow 500 $\mu mol \cdot s^{-1}$, and CO_2 concentration 400 $\mu mol \cdot mol^{-1}$. Measurements were made between 3 to 5 h

after sunrise to ensure similar stomatal aperture between samples. Leaves were left to equilibrate for 2 min in the Li-COR chamber before reading. Leaf PSII fluorescence was measured using a fluorometer using a flash of saturated light (1500 $\mu mol \cdot m^{-2} \cdot s^{-1}$). For plant root surface area (SA) approximations, four sets of plant roots per species were scanned using an EPSON Perfection V19 scanner. The images were processed using *ImageJ* software (v 1.52h) to calculate the 2-D surface area.

Total Ce Association and Translocation: After exposure, plants were harvested, and roots and shoots separated and lyophilized. Dried plant tissue samples were digested overnight at room temperature in concentrated HNO_3 and 30% H_2O_2, then heated to 95 °C for 30 minutes, then allowed to cool down and 30% H_2O_2 was added to obtain a 2:1 HNO_3: H_2O_2 (v/v) ratio and heated again at 95 °C for 2 h (protocol adapted from EPA Method 3050b[53]). Following digestion, the samples were diluted to 5% (v/v) HNO_3 using deionized water and filtered through a 0.45 µm filter before analysis using inductively coupled plasma mass spectrometry (ICP-MS) (Agilent 7700x, Santa Clara, CA). Blanks and standard reference material (Environmental Express, Charleston, SC) were used to validate the digestion and analytical method. The calibration curve consisted of the following concentrations: 0, 1, 10, 50, 100, 500, 1000 µg/kg. All samples either fell within the range of the calibration curve or were diluted to be within the range. Blanks were run every 10 samples. The detection limit was 0.5 µg/kg. Samples were measured five times and averaged to give an output concentration with an RSD.

X-ray Absorption Spectroscopy: After exposure, rinsed roots from two plants were lyophilized, combined, ground and homogenized, pressed into a pellet, and sealed in Kapton® tape. Cerium L_{III} X-ray absorption near edge structure (XANES) spectroscopy data were collected at the Stanford Synchrotron Radiation Lightsource (SSRL) on Beamline 11-2. Beam

energy was calibrated using a Cr foil (5.989 keV). A double crystal monochromator (Si [220], crystal φ=90) equipped with a harmonic rejector was used in conjunction with a 100-element solid-state Ge detector. Measurements were collected at 77 K using a liquid N_2 cryostat. All scans were energy calibrated, deadtime corrected, and averaged using the SIXPACK software package (v1.2.10).[54] Scans were then background subtracted, normalized, and fit using linear combination fitting (LCF) using ATHENA (Demeter v0.9.24).[55] For the purposes of LCF, we assume that the starting materials are all Ce(IV) oxidation state.[56] Ce(III) acetate (Sigma-Aldrich, St. Louis, MO) was used as a model compound for Ce(III).

X-ray fluorescence (XRF) Imaging and μ-XANES Collection and Analysis: After exposure, fresh plant leaves were placed between two pieces of 4 μm-thick Ultralene®, which formed a seal around the plant tissue to minimize dehydration. μ-XRF maps and μ-XANES were acquired at National Synchrotron Light Source (NSLS-II) at Brookhaven National Laboratory on SRX (5-ID) for the CeO_2(0) and CeO_2(−) NP exposures and XFM (4-BM) for the CeO_2(+) NP exposures. On SRX, samples were oriented 45° to incoming beam and to a three-element Vortex-ME3 silicon-drift detector. Elemental maps with an incident energy of 14 keV were collected via fly-scanning using a step size of 4 μm and a dwell time of 0.1 s, and spectral fitting was performed using the PyXRF spectral fitting program.[57] On XFM, samples were oriented 45° to incoming beam and to a four-element Vortex-ME4 silicon-drift detector. Large area (> 1mm) elemental maps with an incident energy of 11 keV were created using a step size of 20 μm and a dwell time of 0.2 s, and spectral fitting was performed using GSE MapViewer in Larch (v 0.9.40).[58] μ-XANES were then collected at locations of interest across the Ce L_{III}-edge (5.623-5.823 keV) and data analysis was performed using ATHENA as detailed above.

RESULTS AND DISCUSSION

NP Characterization: NPs have previously been characterized by transmission electron microscopy (TEM), Fourier-transform infrared spectroscopy (FTIR), and x-ray diffraction (XRD) by Collin et al.[51] The primary crystallite diameters, as measured by TEM, are between 2 and 4 nm. Here, the number-weighted average hydrodynamic diameters of the particles in the exposure medium were 30.3 ± 2.8, 22.9 ± 2.2, and 27.9 ± 2.2 nm for the $CeO_2(+)$, $CeO_2(0)$, and $CeO_2(-)$ particles, respectively. Volume- and intensity- weighted distribution and averages are presented in **Figure S1**. The electrophoretic mobility of the particles in the nutrient solution were +1.69 ± 0.50, −0.14 ± 0.50, and −2.48 ± 0.60 $\mu m \cdot cm \cdot V^{-1} \cdot s^{-1}$ for the $CeO_2(+)$, $CeO_2(0)$, and $CeO_2(-)$ particles, respectively. This corresponds to apparent zeta potentials using the Hückel approximation of +32.2 ± 9.6 mV, −2.6 ± 8.6 mV, and −52.3 ± 12.7 mV, for the $CeO_2(+)$, $CeO_2(0)$, and $CeO_2(-)$ particles, respectively. Generally, a ζ-potential between −10 mV and +10 mV is considered to be relatively neutral, while values greater than ±10 mV to be cationic or anionic, respectively.[59] At the end of the exposure, <0.1% of the Ce remaining in the exposure solution was dissolved (**Table S1**).

Total Ce Uptake: The Ce concentrations associated with plant roots and shoots from the three different treatments are shown in **Figure 1A**. Irrespective of plant species, $CeO_2(+)$ NPs adhered more readily to the plant roots than $CeO_2(-)$ NPs due to electrostatic attraction to the negatively charged root surface or repulsion for the negatively charged particle, which is consistent with numerous other studies comparing the impact of surface charge in plants.[22–25,38,60] Across the plant species, the tomato accumulated the most Ce in/on the roots for all NP treatments, with the

highest being from the CeO_2(+) NP treatment (47,300 ± 3,100 mg/kg). Neutral particles had an intermediate degree of interaction.

The dicots generally show more Ce in the shoots than the monocots (**Figure 1**). This trend is consistent with trends observed by Lopez-Moreno, et al.[61] between dicots (alfalfa, tomato, cucumber) and a monocot (corn) exposed hydroponically to 7 nm CeO_2 NP and by Schwabe et al.[33] between a dicot (pumpkin) and a monocot (wheat) to 9 nm CeO_2 NPs. With regards to surface charge, corn, rice, and lettuce followed previously observed statistically significant trends,[22–24] in which plants accumulated higher amounts of metal in the shoots from the negatively charged NP exposure compared to the positively charged NP exposure. The tomato plant, however, followed the opposite trend, with the highest Ce accumulation from the CeO_2(+) NP treatment and the lowest from the CeO_2(−) NP treatment. This is likely due to high accumulation of Ce in/on the roots from the CeO_2(+) NP exposure compared to the CeO_2(−) NP which enabled more Ce to translocate, albeit less efficiently. The speciation of Ce that is translocating is discussed later in the paper.

Translocation efficiency was also calculated as a ratio of total Ce in shoots to total Ce in/on roots to better compare the capability of different particles to move from the roots to shoots (**Figure 1B**). All plants had the highest translocation efficiencies for the CeO_2(−) NP treatment and the lowest for the CeO_2(+) NP treatment, further suggesting that the positively charged particles adhere too strongly to the root surface to translocate. The CeO_2(−) NP treatment for lettuce had the largest value (24±4 %). Regarding the high Ce leaf concentration in the CeO_2(+) NP exposure in tomato, the lower translocation efficiency for the positive treatment than the negative treatment further corroborates the hypothesis that negatively charged particles are able to more efficiently translocate than positively charged particles. The two dicots translocated Ce

more efficiently than the monocots for all particle types (though the tomato neutral treatment was not statistically significantly higher). This is likely due to the high transpiration rate in the dicots compared to monocots (see later discussion). The trends in uptake observed here for the NPs follow the trends observed in a field study using soil contaminated with Cd, Pb, Cu, and Zn with ten different plants.[62] Lettuce and other leaf vegetables were shown to have higher translocation factors than tomato and other fruit vegetables, which were higher than corn and other grains.

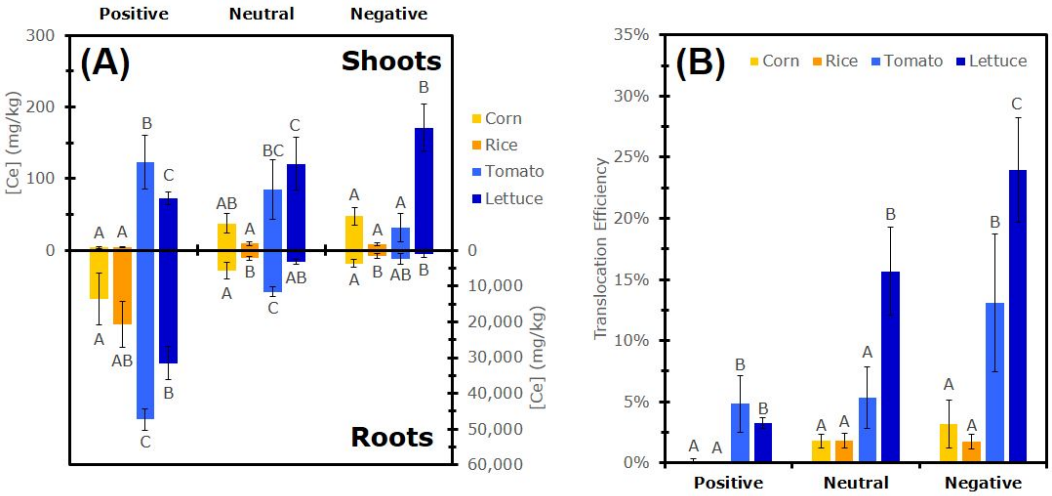

Figure 1. **(A)** Ce concentration (mg-Ce per kg of dried plant tissue) on/in dried roots (bottom) and shoots (top) and **(B)** translocation efficiency (%, Tot Ce_{shoots} / Tot Ce_{roots} of corn (yellow), rice (orange), tomato (light blue), and lettuce (dark blue) after 48 h of hydroponic exposure to 50 mg-Ce/L as CeO_2(+), CeO_2(0), or CeO_2(−) NPs. Roots were rinsed for 30s in Ce-free medium prior to lyophilization and analysis. The means are averaged from four replicates. Error bars correspond to standard deviation. Significant differences [based on ANOVA and Tukey HSD post hoc tests (p<0.05)] between plant species for the same NP treatment for either the roots or shoots are indicated by capital letters.

Calculated root SA for the corn, rice, tomato, and lettuce were 6.6 ± 1.2 cm^2, 0.6 ± 0.2 cm^2, 11.3 ± 3.2 cm^2, and 1.3 ± 1.0 cm^2, respectively (**Table S2**). There was no correlation between root surface area and Ce root uptake/attachment for the CeO_2(+) NP or CeO_2(−) NP exposure (**Figure 2**), emphasizing the importance of this electrostatic attraction/repulsion between the charged NPs and the charged root surface. The roots of dicots generally have greater cation exchange capacities than monocots,[63] which likely explains the higher Ce association for the

tomato and lettuce compared to the corn and rice for the CeO_2(+) NP treatment. In contrast, higher root surface area correlated with higher Ce root attachment/uptake for the CeO_2(0) NP exposure (**Figure 2**), suggesting primarily a sorption interaction when NPs are relatively uncharged.

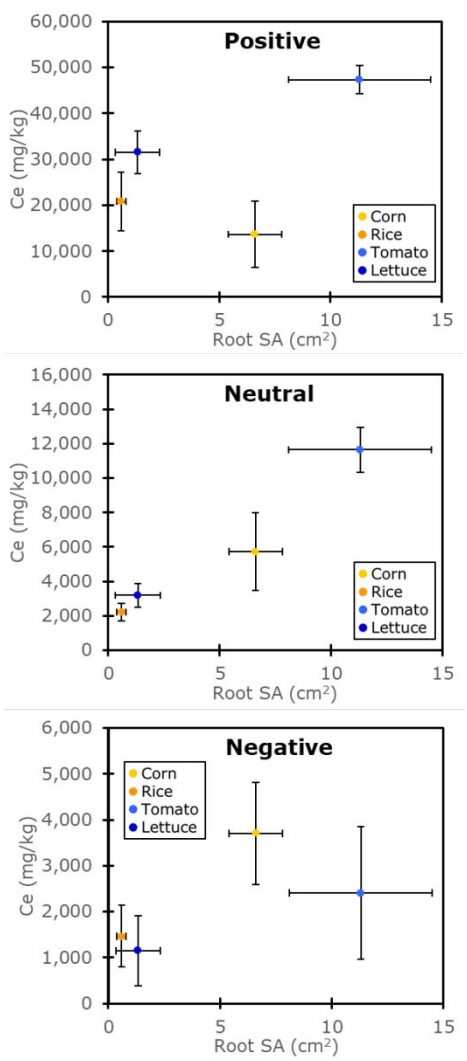

Figure 2. Correlation between root surface area (SA) and Ce associated with roots of corn (yellow), rice (orange), tomato (light blue), and lettuce (dark blue) after 48 h of hydroponic exposure to 50 mg-Ce/L as CeO_2(+), CeO_2(0), or CeO_2(−) NPs. Roots were rinsed for 30s in Ce-free medium prior to lyophilization and analysis. The means are averaged from four replicates. Error bars correspond to standard deviation. Raw values are reported in **Table S2**.

Plant Response: Physiological measurements of plant health are presented in (**Figure 3**). No statistically significant changes in dry biomass were observed for exposed vs. control plants,

likely due to the short-term exposure and low Ce dose. No differences between the exposed and control plants were observed for any of the photosynthesis parameters measured for rice, again likely due to the low Ce transport into its leaves compared to the other plants. In contrast, the most significant changes to plant photosynthesis (*ΦCO₂*, *ΦPSII*, *ETR*) and gas exchange (*E, gsw*) were observed for corn with all NP treatments. Interestingly, similar changes were also observed in the positive NP treatment despite accumulating ~10 times less Ce in the shoots than the neutral and negative NP treatments. We hypothesize that the NPs induce changes to the root water potential, permeability, or conductivity to water. This in turn resulted in a higher stomatal conductance and therefore increased CO_2 uptake and subsequently *ΦPSII*.

For tomato, increases to *ΦCO₂*, *ΦPSII*, *E*, *ETR*, and *gsw* were observed for the CeO_2(0) NP treatment. Negatively charged CeO_2 NPs have been previously reported to boost photosynthesis rates in soil-grown soybean under non-stressed conditions (soil exposure; ζ-potential= −51.57 mV)[64] and salt-stressed canola (hydroponic; ζ-potential= −51.8 mV)[18], and boost carbon assimilation rates and *ΦPSII Arabidopsis* plants exposed to salt-stress, heat, and high light (foliar infiltration; ζ-potential= −17±2.7 mV).[44] Wu et al.[43] observed almost two times higher colocalization of negatively charged (ζ-potential= −16.9±6.1 mV) than neutral/moderately-positive (ζ-potential= +9.7±1.2 mV) CeO_2 NPs within chloroplasts in *Arabidopsis* leaf mesophyll cells exposed via foliar infiltration. Though the observed increase in plant health was not statistically significant for the CeO_2(−) NP treatment, Ce accumulation from this exposure was almost three times lower than from the CeO_2(0) NP exposure. The reported increases in plant photosynthesis by CeO_2(−) NP were observed in stressed Arabidopsis plants experiencing ROS accumulation whereas in this study, plants were exposed to CeO_2 NPs under normal growing conditions. It is likely that oxidative stress levels in tomato were not high enough for

CeO_2 NPs to provide a beneficial impact on plant health through ROS scavenging. In general, the dicots have higher transpiration rates, indicating higher water uptake, which could contribute to their higher Ce uptake.

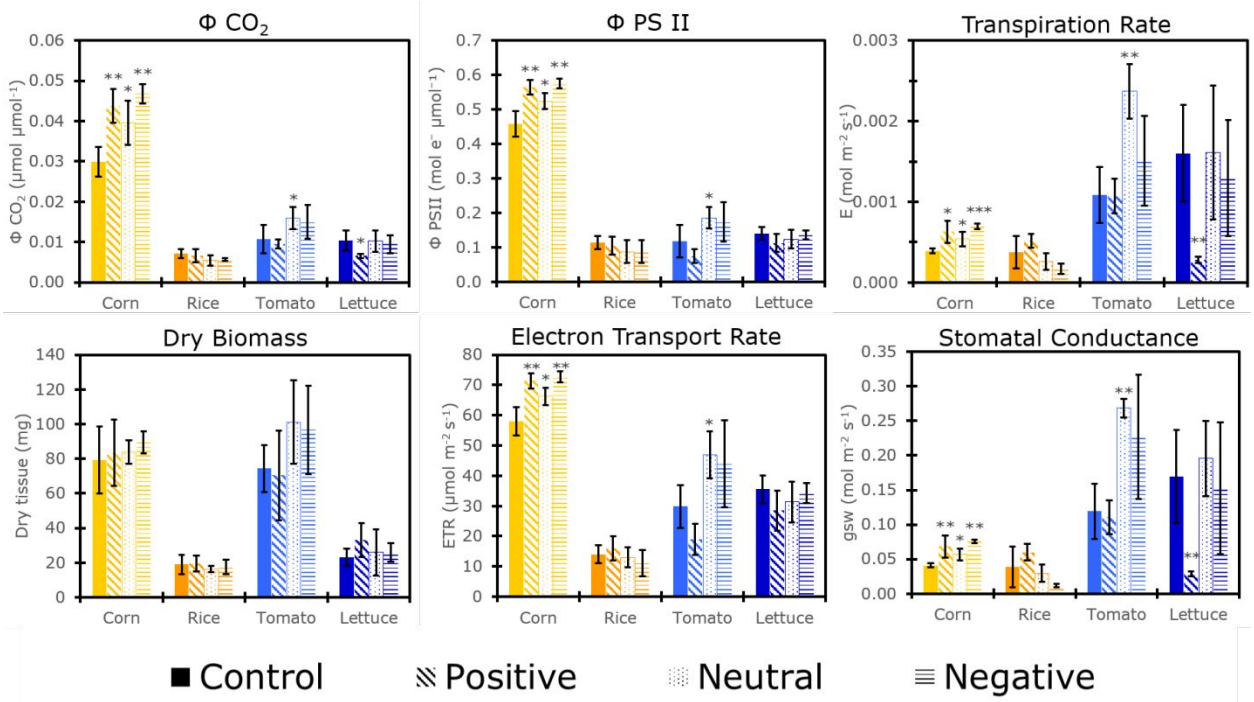

Figure 3. Measurements of quantum yield of CO_2 uptake (ΦCO_2) and photosystem II quantum yield ($\Phi PSII$), transpiration rates (E), dry biomass, electron transport rate (ETR), and stomatal conductance (gsw) after 48 h of hydroponic exposure to 50 mg-Ce/L as CeO_2(+), CeO_2(0), or CeO_2(−) NPs. The means are averaged from four replicates. Error bars correspond to standard deviation. Asterisks indicate statistically significant differences relative to the control (2-sample t-test; * $p \leq 0.05$, ** $p \leq 0.01$).

Negative impacts on ΦCO_2, E, and gsw were observed for the lettuce CeO_2(+) NP exposure. Positively charged CeO_2 NPs (ζ-potential= +32.8±1.0 mV) have been shown to decrease ΦCO_2 and intercellular CO_2 concentration in *Clarkia unguiculata.*[45] Considering ΦCO_2 and not $\Phi PSII$ is impacted, the NPs are likely causing the plant to divert energy for stress response mechanisms rather than the typical plant processes.[65] Cationic NPs in general have been shown to be more toxic in a variety of cells compared to their neutral or anionic counterparts.[51,56,66,67] Asati et al.[67] observed that CeO_2 surface charge influenced toxicity in normal and cancer mammalian cell

lines: positively charged nanoceria would generally localize in lysosomes and release ROS-generating Ce^{3+} due to an acidic microenvironment, while neutral particles localized in the cytoplasm and remained untransformed and displayed no toxicity. In this study, the highest Ce accumulation in leaves from the CeO_2(+) NP treatment was observed in tomato and lettuce, which were the only treatments that observed decreases to plant health, though this decrease was only statistically significant for the lettuce exposure. Lettuce has also been shown to be more sensitive to CeO_2 NPs compared to cabbage, wheat, cucumber, radish, tomato, and rape.[30,68]

Ce Reduction in Roots: No evidence for Ce reduction in/on roots was observed in any plant for the CeO_2(+) NP treatment, while the CeO_2(0) and CeO_2(−) NP treatments show up to ~30% reduction to Ce(III), with the most reduction observed for lettuce. In agreement with these results, previous XANES maps on wheat roots exposed to these same particles show no reduction from the CeO_2(+) NP treatment and ~15% from the CeO_2(0) and CeO_2(−) NP treatments.[22] Furthermore, bulk XANES on hydroponically exposed cucumber (ζ-potential= −10 mV) roots have been shown to undergo some reduction to Ce(III) (<20%).[69–71]

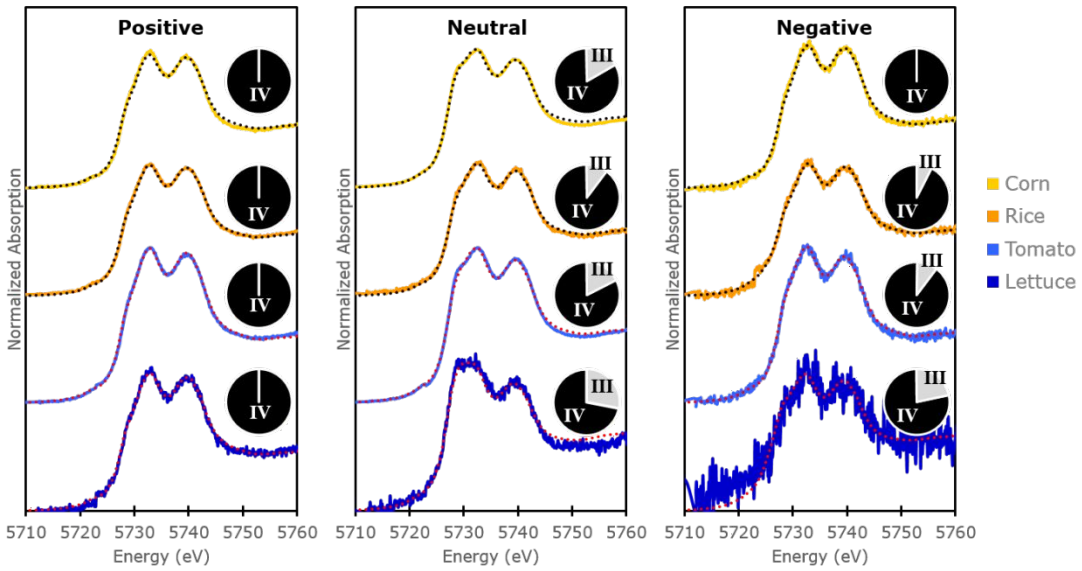

Figure 4. Change in Ce oxidation state, presented as pie charts, in root tissue of corn (yellow), rice (orange), tomato (light blue), and lettuce (dark blue) after 48 h of hydroponic exposure to 50 mg-Ce/L as CeO_2(+), CeO_2(0), or CeO_2(−) NPs. Roots were rinsed for 30s in Ce-free medium prior to lyophilization and analysis. Normalized Ce L_{III} XANES experimental spectra (solid) are presented with LCF fits (dotted). Fitting statistics are provided in **Table S3.**

The exact location of this biotransformation and the mechanisms occurring are still under debate. One hypothesis is that the plant roots are taking up the CeO_2 NPs, after which the NPs undergo reductive dissolution intracellularly to Ce(III), as discussed below. The Ce(III)/Ce(IV) equilibrium mostly involves the atoms on the surface of CeO_2 NPs,[72,73] thus we posit that the Ce(III) is not truly dissolved, but rather that Ce(IV) reduction happens at the NP surface, likely as $CePO_4$. HR-TEM images by Singh et al[74] showed no significant changes to average crystal size of CeO_2 NPs incubated in PBS buffer for 72 h, but the XPS and UV-Vis spectra suggest the formation of amorphous Ce(III) phosphate at the particle surface. This was further corroborated by Schwabe et al.[75] who found less released Ce when phosphate was present in the media, indicating that the Ce(III) is not released from the surface but most likely trapped by the formation of $CePO_4$ on the NP surface. Where majority of the particles remained adhered to the

root outer surface from the CeO_2(+) NP exposure, no reduction was observed, while Ce reduction was observed in the CeO_2(0) and CeO_2(−) NP exposed roots where more particles were likely internalized to a greater degree (as suggested by translocation efficiencies in **Figure 1B**)

However, reductive dissolution at the root surface is also an important mechanism. . Plant roots exude a variety of biomolecules (e.g. organic acids, amino acids) that can promote the dissolution of metal oxide NPs and/or the precipitation of metals.[76,77] It has been proposed that CeO_2 NPs are first reduced then released as Ce(III) with the assistance of reducing substances,[70,78] and then is often precipitated with phosphate.[52,79] Though the particles are stable in solution and do not significantly dissolve (see **Table S2**), CeO_2 NP dissolution has been observed in the presence of low molecular weight organic acids,[37,75] and studies have confirmed both CeO_2 NP and Ce(III) ion uptake in hydroponic exposures by radish,[37] and sunflower, wheat, and pumpkin.[34] Additionally, Schwabe et al.[75] observed greater solution acidification for the dicot (pumpkin) compared to the monocot (wheat) exposed to CeO_2 NPs.

Ce Distribution in Leaves: Both NP charge and plant vasculature affected the distribution of CeO_2 NPs in plant leaves. XFM maps of exposed monocots (corn and rice) are shown in **Figure 5**. For corn, the Ce from the CeO_2(−) NP exposure accumulated in parallel lines with Zn, suggesting the Ce is primarily located in the leaf veins.[80] No Ce fluorescence signal was detected in the leaves of plants for the CeO_2(0) NP treatment. For rice, Ce fluorescence signal from the CeO_2(−) NP treatment formed clusters within the leaf veins as 30% Ce(III). The CeO_2(0) NP treatment in rice induced a non-uniform distribution of Ce; a large aggregate (100 μm x 30 μm) of Ce was detected outside the vasculature. These results are consistent with our previous results in wheat using the same particles where the neutral treatment resulted in clusters outside of the

main vasculature and the negative resulted in Ce accumulation in the veins primarily as Ce(IV) with some reduction (~20%) outside of the vasculature.[22]

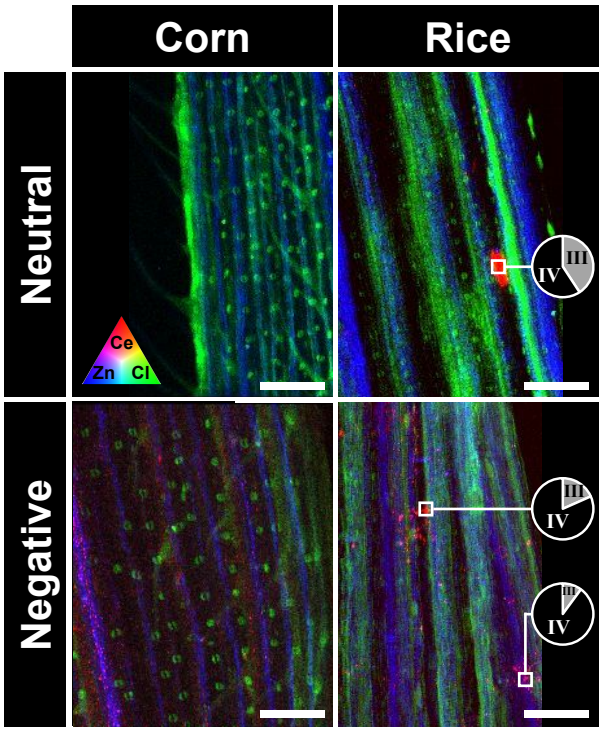

Figure 5. Tri-colored XRF maps of monocot leaves showing Ce (red), Zn (blue), and Cl (green) distribution in corn and rice after 48 h of hydroponic exposure to 50 mg-Ce/L as CeO_2(0) or CeO_2(−) NPs. Ce signal in the leaves exposed to CeO_2(+) NPs was too low for imaging. White boxes indicate where μ-XANES were acquired, with the LCF results presented as a pie chart. Ce signal was too low to acquire μ-XANES for either corn exposure. XRF maps of individual elements and XANES spectra and fitting statistics are provided in **Figures S2-5.** Scale bar=200 μm.

XFM maps of dicots (lettuce and tomato) are shown in **Figures 6-7**. Unlike the monocots, where the Ce was located in small clusters or in the vasculature, Ce is found throughout the leaf. Dicots generally have larger airspace volume than monocots,[81] which may have allowed the Ce to spread further out of the vasculature through the leaf. Previous XRF images of tomato exposed to the same CeO_2(−) NP particles for 14 days showed Ce accumulation within the vascular tissue in relatively large foci as ~40% Ce(III) from the CeO_2(−) NP treatment.[23] Similar accumulation in the primary and secondary veins was observed for tomato CeO_2(−) NP treatment (**Figure S9**),

though less reduction was observed here (13%), possibly due to the shorter exposure period. Interestingly, similar distinct spots were observed in Arabidopsis exposed hydroponically to cationic quantum dots.[82] In contrast, both the lettuce and tomato CeO_2(+) NP exposures showed minimal Ce in the primary vasculature, instead they have Ce clusters around minor veins, suggesting the Ce migrates out of the vasculature at the end of minor veins and accumulates in the cells at this point of exit. Similar Ce accumulation at the leaf tips and at the ends of vascular bundles was observed in cucumber leaves exposed hydroponically to relatively neutral CeO_2 NPs (ζ-potential= 8.8 mV).[83]

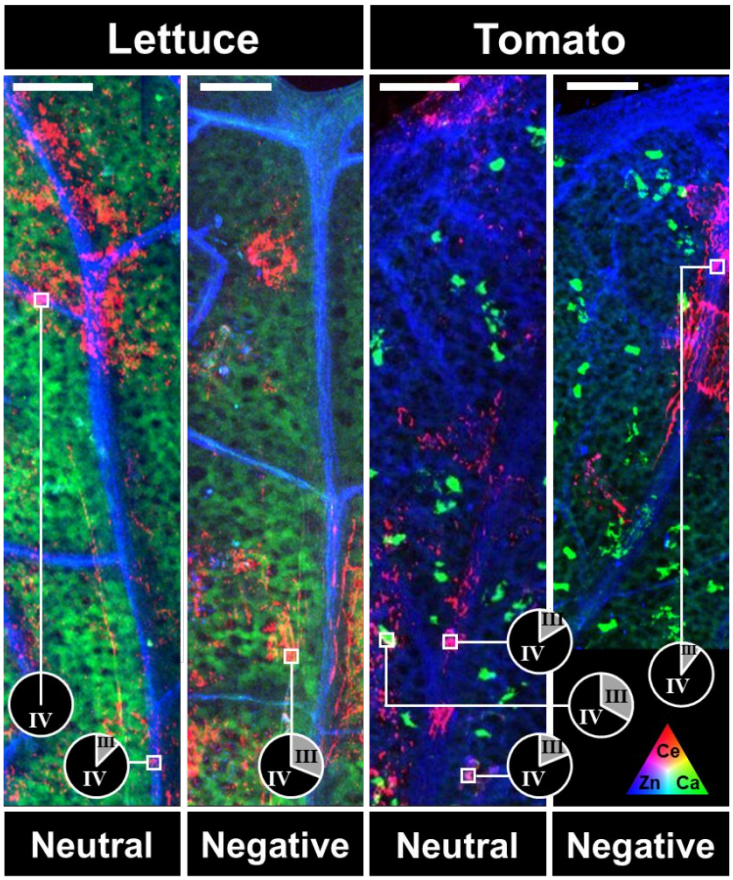

Figure 6. Tri-colored XRF maps of dicot leaves showing Ce (red), Zn (blue), and Ca (green) distribution in lettuce and tomato after 48 h of hydroponic exposure to 50 mg-Ce/L as CeO_2(0), or CeO_2(−) NPs. White boxes indicate where μ-XANES were acquired, with the LCF results presented as a pie chart. XRF maps of individual elements and XANES spectra and fitting statistics are provided in **Figures S6-10.** Scale bar=200 μm.

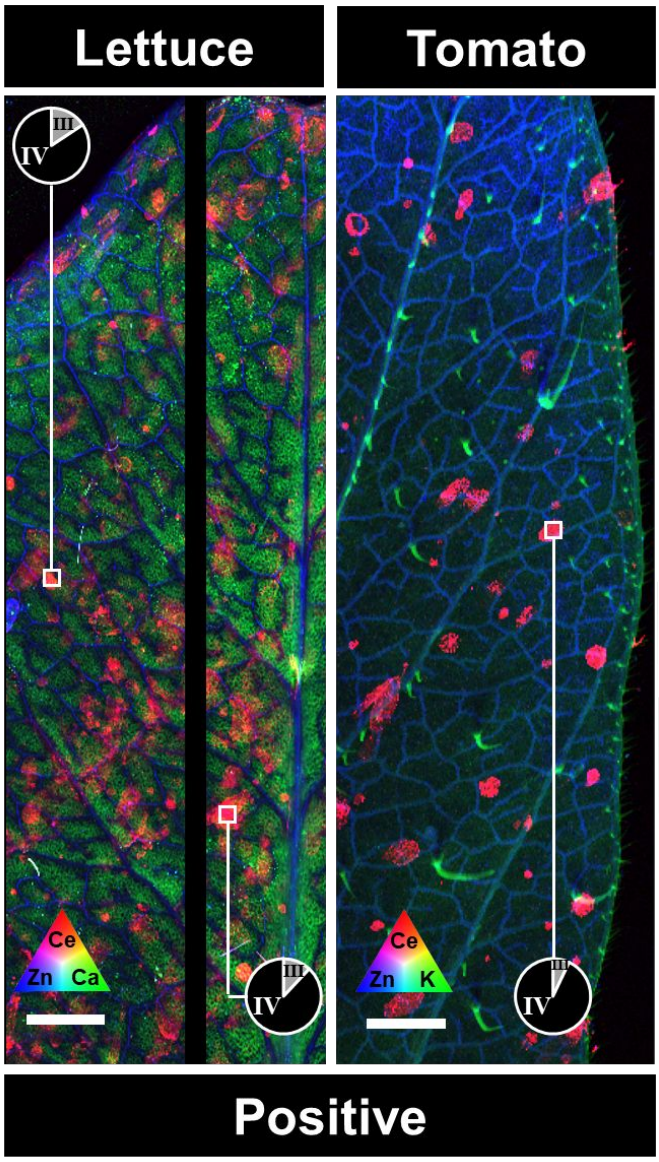

Figure 7. Tri-colored XRF maps of dicot leaves showing Ce (red), Zn (blue), and either Ca (green) for lettuce or K (green) for tomato distribution in lettuce and tomato after 48 h of hydroponic exposure to 50 mg-Ce/L as CeO_2(+). White boxes indicate where μ-XANES were acquired, with the LCF results presented as a pie chart. XRF maps of individual elements and XANES spectra and fitting statistics are provided in **Figures S11-13.** The lettuce map was completed as two scans. Scale bar=1 mm.

In the tomato CeO_2(+) NP exposure in **Figure 7**, there is evidence of Ce-trichome colocalization (see **Figure S14** for larger images of these regions). Trichomes are involved in various secretory and uptake functions, and it has been proposed that metal NPs can be excreted through trichomes.[7] Many types of trichomes have been shown to accumulate internalized or

airborne metals as a detoxification mechanism.[84,85] With specific regards to NPs, trichomes have been shown to accumulate various types of NPs, including C-coated nano-Fe_xO_y,[86] nano- TiO_2,[87] and nano-gold.[6] Thus, the CeO_2 NPs could have been translocated from the roots to the shoots through the vascular tissue before being sequestered in the trichomes of the leaves to be further exuded from the plant.

CONCLUSIONS

Both surface chemistry and plant species have a significant impact on the uptake and distribution of CeO_2 NPs. Positively charged CeO_2 NPs remained primarily adhered to the negatively charged roots via electrostatics as Ce(IV), with poor Ce translocation efficiency to the shoots. In contrast, negatively charged CeO_2 NPs accumulated significantly less on the roots but had the highest translocation efficiency. Overall, tomato and lettuce (dicots) were able to translocate Ce more efficiently to the shoots than rice and corn. This correlates with higher transpiration rates, and thus water uptake. Increases in plant photosynthesis were observed in corn plants exposed to CeO_2 NPs of all charges that were accompanied by enhanced stomatal aperture and therefore CO_2 uptake. In contrast some reduction to plant photosynthesis was observed in plants under CeO_2(+) NP exposure, potentially a result of the different spatial distribution of the CeO_2(+) NPs in the leaves. Once in the leaves, CeO_2(−) remained primarily in the veins, while (0) and (+) formed clusters outside of the vasculature, possibly because of different surface biotransformation *in planta* (e.g. corona formation, heteroaggregation), and/or differential potential for membrane crossing conferred by charge type and/or density. Further research is needed to understand why NPs with surfaces of different charges showed such a different leaf distribution. All in all these results indicates that, even if influenced by plant

morphologies, tuning NP surface charge can allow NPs targeting to different plant compartment following root uptake. The different Ce distribution as a function of particle surface chemistry suggests that NPs may potentially be engineered for targeted, NP mediated delivery of agrochemicals to different plant organs.

ACKNOWLEDGEMENTS

This material is based upon work supported by the U.S. National Science Foundation (NSF) and the Environmental Protection Agency (EPA) under NSF Cooperative Agreement EF-1266252, Center for the Environmental Implications of NanoTechnology (CEINT), Nano for Agriculturally Relevant Materials (NanoFARM) (CBET-1530563), and from the NSF Integrated Graduate Education and Research Traineeship Nanotechnology Environmental Effects and Policy (IGERT-NEEP) (DGE-0966227). Parts of this research used the XFM and SRX Beamlines of the National Synchrotron Light Source II, a U.S. Department of Energy (DOE) Office of Science User Facility operated for the DOE Office of Science by Brookhaven National Laboratory under Contract No. DE-SC0012704. A.S.A was supported by a DOE-Geosciences Grant (DE-FG02-92ER14244). We thank J. Thieme for his help running the SRX beamline at NSLS-II. Bulk XAS on root tissue was performed on Beamline 11-2 at the Stanford Synchrotron Radiation Lightsource (SSRL). We thank Jieran Li for synthesis of the NPs.

REFERENCES

1 S. M. Rodrigues, P. Demokritou, N. Dokoozlian, C. O. Hendren, B. Karn, M. S. Mauter, O. A. Sadik, M. Safarpour, J. M. Unrine, J. Viers, P. Welle, J. C. White, M. R. Wiesner and G. V. Lowry, Nanotechnology for Sustainable Food Production: Promising opportunities and scientific challenges, *Environ. Sci. Nano*, 2017, **7**, 899–904.

2 A. D. Servin, W. H. Elmer, A. Mukherjee, R. De La Torre-Roche, H. Hamdi, J. C. White, P. S. Bindraban and C. O. Dimkpa, A review of the use of engineered nanomaterials to

suppress plant disease and enhance crop yield, *J. Nanoparticle Res.*, 2015, **17**, 92.

3 M. Kah, S. Beulke, K. Tiede and T. Hofmann, Nanopesticides: State of Knowledge, Environmental Fate, and Exposure Modeling, *Crit. Rev. Environ. Sci. Technol.*, 2013, **43**, 1823–1867.

4 P. Wang, E. Lombi, F.-J. Zhao and P. M. Kopittke, Nanotechnology: A New Opportunity in Plant Sciences, *Trends Plant Sci.*, 2016, **21**, 699–712.

5 X. Zhao, H. Cui, Y. Wang, C. Sun, B. Cui and Z. Zeng, Development Strategies and Prospects of Nano-based Smart Pesticide Formulation, *J. Agric. Food Chem.*, 2017, **66**, 6504–6512.

6 A. Avellan, J. Yun, Y. Zhang, E. Spielman-Sun, J. M. Unrine, J. Thieme, J. Li, E. Lombi, G. Bland and G. V. Lowry, Nanoparticle Size and Coating Chemistry Control Foliar Uptake Pathways, Translocation, and Leaf-to-Rhizosphere Transport in Wheat, *ACS Nano*, 2019, acsnano.8b09781.

7 F. Schwab, G. Zhai, M. Kern, A. Turner, J. L. Schnoor and M. R. Wiesner, Barriers , pathways and processes for uptake , translocation and accumulation of nanomaterials in plants – Critical review, *Nanotoxicology*, 2015, **10**, 257–278.

8 W. Du, W. Tan, J. R. Peralta-Videa, J. L. Gardea-Torresdey, R. Ji, Y. Yin and H. Guo, Interaction of metal oxide nanoparticles with higher terrestrial plants: Physiological and biochemical aspects., *Plant Physiol. Biochem.*, 2017, **110**, 210–225.

9 W. H. De Jong and P. J. A. Borm, Drug delivery and nanoparticles: Applications and hazards, *Int. J. Nanomedicine*, 2008, **3**, 133–149.

10 P. González-Melendi, R. Fernández-Pacheco, M.-J. Coronado, E. Corredor, P. S. Testillano, M. C. Risueño, C. Marquina, M. R. Ibarra, D. Rubiales and A. Pérez-de-Luque, Nanoparticles as smart treatment-delivery systems in plants: Assessment of different techniques of microscopy for their visualization in plant tissues, *Ann. Bot.*, 2008, **101**, 187–195.

11 X. Gao, A. Avellan, S. N. Laughton, R. Vaidya, S. M. Rodrigues, E. A. Casman and G. V. Lowry, CuO nanoparticle dissolution and toxicity to wheat (Triticum aestivum) in rhizosphere soil, *Environ. Sci. Technol.*, 2018, **52**, 2888–2897.

12 E. Spielman-Sun, E. Lombi, E. Donner, A. Avellan, D. L. Howard, B. Etschmann, D. L. Howard and G. V. Lowry, Temporal evolution of copper distribution and speciation in roots of Triticum aestivum exposed to CuO, Cu(OH)2, and CuS nanoparticles., *Environ. Sci. Technol.*, 2018, **52**, 9777–9784.

13 I. Iavicoli, V. Leso, D. H. Beezhold and A. A. Shvedova, Nanotechnology in agriculture: Opportunities, toxicological implications, and occupational risks, *Toxicol. Appl. Pharmacol.*, 2017, **329**, 96–111.

14 J. P. Giraldo, M. P. Landry, S. M. Faltermeier, T. P. Mcnicholas, N. M. Iverson, A. A. Boghossian, N. F. Reuel, A. J. Hilmer, F. Sen, J. A. Brew and M. S. Strano, Plant nanobionics approach to augment photosynthesis and biochemical sensing, *Nat. Mater.*, 2014, **13**, 400–408.

15 S. Arora, P. Sharma, S. Kumar, R. Nayan, P. K. Khanna and M. G. H. Zaidi, Gold-nanoparticle induced enhancement in growth and seed yield of Brassica juncea, *Plant Growth Regul.*, 2012, **66**, 303–310.

16 R. Raliya, R. Nair, S. Chavalmane, W.-N. Wang and P. Biswas, Mechanistic evaluation of translocation and physiological impact of titanium dioxide and zinc oxide nanoparticles on the tomato (Solanum lycopersicum L.) plant, *Metallomics*, 2015, **7**, 1584–1594.

17 J. Hong, L. Wang, Y. Sun, L. Zhao, G. Niu, W. Tan, C. M. Rico, J. R. Peralta-Videa and J. L. Gardea-Torresdey, Foliar applied nanoscale and microscale CeO2 and CuO alter cucumber (Cucumis sativus) fruit quality, *Sci. Total Environ.*, 2016, **563–564**, 904–911.
18 L. Rossi, W. Zhang, L. L. Lombardini and X. Ma, The impact of cerium oxide nanoparticles on the salt stress responses of brassica napus L., *Environ. Pollut.*, 2016, **219**, 28–36.
19 W. H. Elmer and J. C. White, The use of metallic oxide nanoparticles to enhance growth of tomatoes and eggplants in disease infested soil or soilless medium, *Environ. Sci. Nano*, 2016, **3**, 1072–1079.
20 P. Ponmurugan, K. Manjukarunambika, V. Elango and B. M. Gnanamangai, Antifungal activity of biosynthesised copper nanoparticles evaluated against red root-rot disease in tea plants, *J. Exp. Nanosci.*, 2016, **11**, 1019–1031.
21 S. Bandyopadhyay, K. Ghosh and C. Varadachari, Multimicronutrient Slow-Release Fertilizer of Zinc, Iron, Manganese, and Copper, *Int. J. Chem. Eng.*, 2014, **2014**, 1–7.
22 E. Spielman-Sun, E. Lombi, E. Donner, D. L. Howard, J. M. Unrine and G. V. Lowry, Impact of surface charge on cerium oxide nanoparticle uptake and translocation by wheat (Triticum aestivum), *Environ. Sci. Technol.*, 2017, **51**, 7361–7368.
23 J. Li, R. V Tappero, A. S. Acerbo, H. Yan, Y. Chu, G. V. Lowry and J. M. Unrine, Effect of CeO2 nanomaterial surface functional groups on tissue and subcellular distribution of Ce in tomato (Solanum lycopersicum), *Environ. Sci. Nano*, 2018, **6**, 273–285.
24 Z.-J. Zhu, H. Wang, B. Yan, H. Zheng, Y. Jiang, O. R. Miranda, V. M. Rotello, B. Xing and R. W. Vachet, Effect of surface charge on the uptake and distribution of gold nanoparticles in four plant species., *Environ. Sci. Technol.*, 2012, **46**, 12391–8.
25 H. Li, X. Ye, X. Guo, Z. Geng and G. Wang, Effects of surface ligands on the uptake and transport of gold nanoparticles in rice and tomato, *J. Hazard. Mater.*, 2016, **314**, 188–196.
26 A. Albanese, P. S. Tang and W. C. W. Chan, The Effect of Nanoparticle Size, Shape, and Surface Chemistry on Biological Systems, *Annu. Rev. Biomed. Eng*, 2012, **14**, 1–16.
27 T. T. S. Lew, M. H. Wong, S. Y. Kwak, R. Sinclair, V. B. Koman and M. S. Strano, Rational Design Principles for the Transport and Subcellular Distribution of Nanomaterials into Plant Protoplasts, *Small*, 2018, **14**, 1–13.
28 C. M. Rico, M. G. Johnson, M. A. Marcus and C. P. Andersen, Shifts in N and δ15N in wheat and barley exposed to cerium oxide nanoparticles, *NanoImpact*, 2018, **11**, 156–163.
29 J. D. Judy, J. M. Unrine, W. Rao, S. Wirick and P. M. Bertsch, Bioavailability of gold nanomaterials to plants: Importance of particle size and surface coating, *Environ. Sci. Technol.*, 2012, **46**, 8467–8474.
30 Y. Ma, L. Kuang, X. He, W. Bai, Y. Ding, Z. Zhang, Y. Zhao and Z. Chai, Effects of rare earth oxide nanoparticles on root elongation of plants, *Chemosphere*, 2010, **78**, 273–279.
31 P. Wang, E. Lombi, S. Sun, K. G. Scheckel, A. Malysheva, B. A. McKenna, N. W. Menzies, F.-J. Zhao and P. M. Kopittke, Characterizing the uptake, accumulation and toxicity of silver sulfide nanoparticles in plants, *Environ. Sci. Nano*, 2017, **4**, 448–460.
32 D. Sun, H. I. H. I. Hussain, Z. Yi, R. Siegele, T. Cresswell, L. Kong and D. M. D. M. Cahill, Uptake and cellular distribution, in four plant species, of fluorescently labeled mesoporous silica nanoparticles, *Plant Cell Rep.*, 2014, **33**, 1389–1402.
33 F. Schwabe, R. Schulin, L. K. Limbach, W. Stark, D. Bürge and B. Nowack, Influence of two types of organic matter on interaction of CeO2 nanoparticles with plants in hydroponic culture, *Chemosphere*, 2013, **91**, 512–520.

34 F. Schwabe, S. Tanner, R. Schulin, A. Rotzetter, W. Stark, A. Von Quadt and B. Nowack, Dissolved cerium contributes to uptake of Ce in the three crop plants, *Metallomics*, 2015, **7**, 466–477.
35 W. Zhang, S. D. Ebbs, C. Musante, J. C. White, C. Gao and X. Ma, Uptake and Accumulation of Bulk and Nanosized Cerium Oxide Particles and Ionic Cerium by Radish (*Raphanus sativus* L.), *J. Agric. Food Chem.*, 2015, **63**, 382–390.
36 L. Rossi, W. Zhang, A. P. Schwab and X. Ma, Uptake, accumulation and in-planta distribution of co-existing cerium oxide nanoparticles and cadmium in Glycine max (L.) Merr., *Environ. Sci. Technol.*, 2017, **51**, 12815–12824.
37 W. Zhang, Y. Dan, H. Shi and X. Ma, Elucidating the mechanisms for plant uptake and in-planta speciation of cerium in radish (Raphanus sativus L.) treated with cerium oxide nanoparticles, *J. Environ. Chem. Eng.*, 2017, **5**, 572–577.
38 A. Avellan, F. Schwab, A. Masion, P. Chaurand, D. Borschneck, V. Vidal, J. Rose, C. Santaella and C. Levard, Nanoparticle Uptake in Plants: Gold Nanomaterial Localized in Roots of Arabidopsis thaliana by X-ray Computed Nanotomography and Hyperspectral Imaging, *Environ. Sci. Technol.*, 2017, **51**, 8682–8691.
39 Y. Xue, Q. Luan, D. Yang, X. Yao and K. Zhou, Direct evidence for hydroxyl radical scavenging activity of cerium oxide nanoparticles, *J. Phys. Chem. C*, 2011, **115**, 4433–4438.
40 R. W. Tarnuzzer, J. Colon, S. Patil and S. Seal, Vacancy engineered ceria nanostructures for protection from radiation-induced cellular damage, *Nano Lett.*, 2005, **5**, 2573–2577.
41 T. Pirmohamed, J. M. Dowding, S. Singh, B. Wasserman, E. Heckert, A. S. Karakoti, J. E. S. King, S. Seal and W. T. Self, Nanoceria exhibit redox state-dependent catalase mimetic activity, *Chem. Commun.*, 2010, **46**, 2736–2738.
42 A. A. Boghossian, F. Sen, B. M. Gibbons, S. Sen, S. M. Faltermeier, J. P. Giraldo, C. T. Zhang, J. Zhang, D. A. Heller and M. S. Strano, Application of nanoparticle antioxidants to enable hyperstable chloroplasts for solar energy harvesting, *Adv. Energy Mater.*, 2013, **3**, 881–893.
43 H. Wu, N. Tito and J. P. Giraldo, Anionic Cerium Oxide Nanoparticles Protect Plant Photosynthesis from Abiotic Stress by Scavenging Reactive Oxygen Species, *ACS Nano*, 2017, **11**, 11283–11297.
44 H. Wu, L. Shabala, S. Shabala and J. P. Giraldo, Hydroxyl radical scavenging by cerium oxide nanoparticles improves Arabidopsis salinity tolerance by enhancing leaf mesophyll potassium retention, *Environ. Sci. Nano*, 2018, **5**, 1567–1583.
45 J. R. Conway, A. L. Beaulieu, N. L. Beaulieu, S. J. Mazer and A. A. Keller, Environmental Stresses Increase Photosynthetic Disruption by Metal Oxide Nanomaterials in a Soil-Grown Plant, *ACS Nano*, 2015, **9**, 11737–11749.
46 L. Zhao, B. Peng, J. A. Hernandez-Viezcas, C. M. Rico, Y. Sun, J. R. Peralta-Videa, X. Tang, G. Niu, L. Jin, A. Varela-Ramirez, J.-Y. Zhang and J. L. Gardea-Torresdey, Stress response and tolerance of Zea mays to CeO2 nanoparticles: Cross talk among H2O2, heat shock protein, and lipid peroxidation, *ACS Nano*, 2012, **6**, 9615–9622.
47 Z. Cao, C. Stowers, L. Rossi, W. Zhang, L. Lombardini and X. Ma, Physiological effects of cerium oxide nanoparticles on the photosynthesis and water use efficiency of soybean (: Glycine max (L.) Merr.), *Environ. Sci. Nano*, 2017, **4**, 1086–1094.
48 A. C. Barrios, I. A. Medina-Velo, N. Zuverza-Mena, O. E. Dominguez, J. R. Peralta-Videa and J. L. Gardea-Torresdey, *Plant Physiol. Biochem.*, 2016, 110, 100–107.

49 X. Gui, Z. Zhang, S. Liu, Y. Ma, P. Zhang, X. He, Y. Li, J. Zhang, H. Li, Y. Rui, L. Liu and W. Cao, Fate and phytotoxicity of CeO2 nanoparticles on lettuce cultured in the potting soil environment, *PLoS One*, 2015, **10**, 1–10.

50 G. Pulido-Reyes, I. Rodea-Palomares, S. Das, T. S. Sakthivel, F. Leganes, R. Rosal, S. Seal and F. Fernández-Pinãs, Untangling the biological effects of cerium oxide nanoparticles: The role of surface valence states, *Sci. Rep.*, 2015, **5**, 15613.

51 B. E. Collin, E. K. Oostveen, O. V. Tsyusko and J. M. Unrine, Influence of Natural Organic Matter and Surface Charge on the Toxicity and Bioaccumulation of Functionalized Ceria Nanoparticles in Caenorhabditis elegans, *Environ. Sci. Technol.*, 2014, **48**, 1280–1289.

52 P. Zhang, Y. Ma, C. Xie, Z. Guo, X. He, E. Valsami-Jones, I. Lynch, W. Luo, L. Zheng and Z. Zhang, Plant Species Dependent Transformation and Translocation of Ceria Nanoparticles, *Environ. Sci. Nano*, 2019, **6**, 60–67.

53 United States Environmental Protection Agency, Method 3050B - Acid digestion of sediments, sludges, and soils., *Method 3050B*, , DOI:10.1117/12.528651.

54 S. M. Webb, SIXPack a Graphical User Interface for XAS Analysis Using IFEFFIT, *Phys. Scr.*, 2005, **T115**, 1011–1014.

55 B. Ravel and M. Newville, ATHENA, ARTEMIS, HEPHAESTUS: Data analysis for X-ray absorption spectroscopy using IFEFFIT, *J. Synchrotron Radiat.*, 2005, **12**, 537–541.

56 U. M. Graham, M. T. Tseng, J. B. Jasinski, R. A. Yokel, J. M. Unrine, B. H. Davis, A. K. Dozier, S. S. Hardas, R. Sultana, E. A. Grulke and D. A. Butterfield, In vivo processing of ceria nanoparticles inside liver: Impact on free-radical scavenging activity and oxidative stress, *Chempluschem*, 2014, **79**, 1083–1088.

57 H. Yan, W. Xu, D. Yu, A. Heroux, W.-K. Lee, L. Li, S. Campbell and Y. Chu, PyXRF: Python-based X-ray fluorescence analysis package, *X-Ray Nanoimaging Instruments Methods III*, 2017, 30.

58 M. Newville, in *Journal of Physics: Conference Series*, IOP Publishing, 2013, vol. 430, p. 012007.

59 G. V. Lowry, R. J. Hill, S. Harper, A. F. Rawle, C. O. Hendren, F. Klaessig, U. Nobbmann, P. Sayre and J. Rumble, Guidance to improve the scientific value of zeta-potential measurements in nanoEHS, *Environ. Sci. Nano*, 2016, **3**, 953–965.

60 J. Wang, Y. Yang, H. Zhu, J. Braam, J. L. Schnoor and P. J. J. Alvarez, Uptake, Translocation, and Transformation of Quantum Dots with Cationic versus Anionic Coatings by Populus deltoides × nigra Cuttings, *Environ. Sci. Technol.*, 2014, **48**, 6754–6762.

61 M. L. Lopez-Moreno, G. de la Rosa, J. A. Hernandez-Viezcas, H. Castillo-Michel, C. E. Botez, J. R. Peralta-Videa and J. L. Gardea-Torresdey, Evidence of the Differential Biotransformation and Genotoxicity of ZnO and CeO2Nanoparticles on Soybean (Glycine max) Plants, *Environ. Sci. Technol.*, 2010, **44**, 7315–7320.

62 N. Mirecki, R. Agič, L. Šunić, L. Milenković and Z. S. Ilić, Transfer factor as indicator of heavy metals content in plants, *Fresenius Environ. Bull.*, 2015, **24**, 4212–4219.

63 W. M. Crooke, The measurement of the cation-exchange capacity of plant roots, *Plant Soil*, 1964, **21**, 43–49.

64 Z. Cao, L. Rossi, C. Stowers, W. Zhang, L. Lombardini and X. Ma, The impact of cerium oxide nanoparticles on the physiology of soybean (Glycine max (L.) Merr.) under different soil moisture conditions, *Environ. Sci. Pollut. Res.*, 2018, **25**, 930–939.

65 S. D. Loriaux, T. J. Avenson, J. M. Welles, D. K. Mcdermitt, R. D. Eckles, B. Riensche and B. Genty, Closing in on maximum yield of chlorophyll fluorescence using a single multiphase flash of sub-saturating intensity, *Plant, Cell Environ.*, 2013, **36**, 1755–1770.
66 Z. V. Feng, I. L. Gunsolus, T. A. Qiu, K. R. Hurley, L. H. Nyberg, H. Frew, K. P. Johnson, A. M. Vartanian, L. M. Jacob, S. E. Lohse, M. D. Torelli, R. J. Hamers, C. J. Murphy and C. L. Haynes, Impacts of gold nanoparticle charge and ligand type on surface binding and toxicity to Gram-negative and Gram-positive bacteria, *Chem. Sci.*, 2015, **6**, 5186–5196.
67 A. Asati, S. Santra, C. Kaittanis and J. M. Perez, Surface-charge-dependent cell localization and cytotoxicity of cerium oxide nanoparticles, *ACS Nano*, 2010, **4**, 5321–5331.
68 P. Zhang, Y. Ma, Z. Zhang, X. He, Y. Li, J. Zhang, L. Zheng and Y. Zhao, Species-specific toxicity of ceria nanoparticles to Lactuca plants, *Nanotoxicology*, 2015, **9**, 1–8.
69 Y. Ma, X. He, P. Zhang, Z. Zhang, Y. Ding, J. Zhang, G. Wang, C. Xie, W. Luo, J. Zhang, J. Zhang, L. Zheng, Z. Chai and K. Yang, Xylem and Phloem Based Transport of CeO 2 Nanoparticles in Hydroponic Cucumber Plants, *Environ. Sci. Technol.*, 2017, **51**, 5215–5221.
70 P. Zhang, Y. Ma, Z. Zhang, X. He, J. Zhang, Z. Guo, R. Tai, Y. Zhao and Z. Chai, Biotransformation of Ceria Nanoparticles in Cucumber Plants, *ACS Nano*, 2012, **6**, 9943–9950.
71 P. Zhang, C. Xie, Y. Ma, X. He, Z. Zhang, Y. Ding, L. Zheng and J. Zhang, Shape-Dependent Transformation and Translocation of Ceria Nanoparticles in Cucumber Plants, *Environ. Sci. Technol. Lett.*, 2017, **4**, 380–385.
72 M. Baalousha, P. Le Coustumer, I. Jones and J. R. Lead, Characterisation of structural and surface speciation of representative commercially available cerium oxide nanoparticles, *Environ. Chem.*, 2010, **7**, 377–385.
73 L. Wu, H. J. Wiesmann, A. R. Moodenbaugh, R. F. Klie, Y. Zhu, D. O. Welch and M. Suenaga, Oxidation state and lattice expansion of CeO2-x nanoparticles as a function of particle size, *Phys. Rev. B*, 2004, **69**, 125415.
74 S. Singh, T. Dosani, A. S. Karakoti, A. Kumar, S. Seal and W. T. Self, A phosphate-dependent shift in redox state of cerium oxide nanoparticles and its effects on catalytic properties, *Biomaterials*, 2011, **32**, 6745–6753.
75 F. Schwabe, R. Schulin, P. Rupper, A. Rotzetter, W. Stark and B. Nowack, Dissolution and transformation of cerium oxide nanoparticles in plant growth media, *J. Nanoparticle Res.*, 2014, **16**, 2668.
76 J. Lv, S. Zhang, L. Luo, J. Zhang, K. Yang and P. Christie, Accumulation, speciation and uptake pathway of ZnO nanoparticles in maize, *Environ. Sci. Nano*, 2015, **2**, 68–77.
77 P. Zhang, Y. Ma, Z. Zhang, X. He, Z. Guo, R. Tai, Y. Ding, Y. Zhao and Z. Chai, Comparative toxicity of nanoparticulate/bulk Yb 2O 3 and YbCl 3 to cucumber (Cucumis sativus), *Environ. Sci. Technol.*, 2012, **46**, 1834–1841.
78 Y. Ma, P. Zhang, Z. Zhang, X. He, J. Zhang, Y. Ding, J. Zhang, L. Zheng, Z. Guo, L. Zhang, Z. Chai and Y. Zhao, Where Does the Transformation of Precipitated Ceria Nanoparticles in Hydroponic Plants Take Place?, *Environ. Sci. Technol.*, 2015, **49**, 10667–10674.
79 G. Wang, Y. Ma, P. Zhang, X. He, Z. Zhang, M. Qu, Y. Ding, J. Zhang, C. Xie, W. Luo, J. Zhang, S. Chu, Z. Chai and Z. Zhang, Influence of phosphate on phytotoxicity of ceria

nanoparticles in an agar medium, *Environ. Pollut.*, 2017, **224**, 392–399.
80 P. M. Kopittke, T. Punshon, D. J. Paterson, R. V Tappero, P. Wang, F. P. C. Blamey, A. van der Ent and E. Lombi, Synchrotron-Based X-Ray Fluorescence Microscopy as a Technique for Imaging of Elements in Plants, *Plant Physiol.*, 2018, **178**, 507–523.
81 G. S. Byott, Leaf air space systems in C3 and C4 species, *New Phytol.*, 1976, **76**, 295–299.
82 Y. Koo, J. Wang, Q. Zhang, H. Zhu, E. W. Chehab, V. L. Colvin, P. J. J. Alvarez and J. Braam, Fluorescence reports intact quantum dot uptake into roots and translocation to leaves of arabidopsis thaliana and subsequent ingestion by insect herbivores, *Environ. Sci. Technol.*, 2015, **49**, 626–632.
83 Z. Zhang, X. He, H. Zhang, Y. Ma, P. Zhang, Y. Ding and Y. Zhao, Uptake and distribution of ceria nanoparticles in cucumber plants., *Metallomics*, 2011, **3**, 816–822.
84 G. Gutierrez-Alcala, C. Gotor, A. J. Meyer, M. Fricker, J. M. Vega and L. C. Romero, Glutathione biosynthesis in Arabidopsis trichome cells., *Proc. Natl. Acad. Sci. U. S. A.*, 2000, **97**, 11108–13.
85 Y.-E. Choi, E. Harada, M. Wada, H. Tsuboi, Y. Morita, T. Kusano and H. Sano, Detoxification of cadmium in tobacco plants: Formation and active excretion of crystals containing cadmium and calcium through trichomes, *Planta*, 2001, **213**, 45–50.
86 E. Corredor, P. S. Testillano, M.-J. Coronado, P. González-Melendi, R. Fernández-Pacheco, C. Marquina, M. R. Ibarra, J. M. De La Fuente, D. Rubiales, A. Pérez-de-Luque and M.-C. Risueño, Nanoparticle penetration and transport in living pumpkin plants: in situ subcellular identification, *BMC Plant Biol.*, 2009, **9**, 45.
87 A. D. Servin, H. Castillo-Michel, J. A. Hernandez-Viezcas, B. C. Diaz, J. R. Peralta-Videa and J. L. Gardea-Torresdey, Synchrotron micro-XRF and micro-XANES confirmation of the uptake and translocation of TiO2 nanoparticles in cucumber (Cucumis sativus) plants, *Environ. Sci. Technol.*, 2012, **46**, 7637–7643.

TOC ART

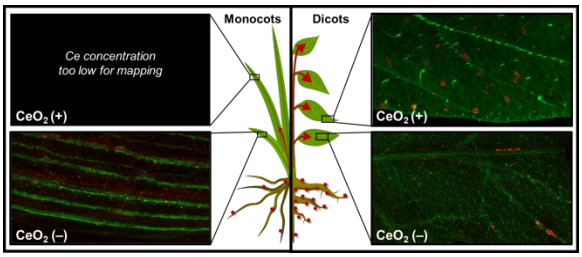
Monocots
Dicots
Ce concentration
too low for mapping
CeO2 (+)
CeO2 (+)
CeO2 (–)
CeO2 (–)